buildings

MDPI

Article

Optimization of Cast-Steel Tubular Circular-Hollow-Section Connections Based on Depth-First Search Algorithm

Kaien Jiang [1], Ziming Yang [2], Ju Chen [2,*], Guoer Lv [1] and Huafeng Yu [1]

[1] Power China Huadong Engineering Corporation Limited, Hangzhou 310014, China; jiang_ke@hdec.com (K.J.); lv_ge@hdec.com (G.L.); yu_hf@hdec.com (H.Y.)
[2] Institute of Structural Engineering, Zhejiang University, Hangzhou 310058, China; yangziming@zju.edu.cn
* Correspondence: cecj@zju.edu.cn

Abstract: This study introduces a novel design for a cast-steel joint in the shape of a T, aimed at resolving concerns regarding stress concentration at points where geometric intersections occur and enhancing the quality of welding in T-shaped welded joints. The proposed integrated design framework greatly facilitated the successful construction of a three-dimensional joint between a brace and a chord at a T-shaped node. The geometric parameters of curves in the connector were optimized using a depth-first search algorithm, resulting in control points for the optimized curve. Computer-aided design software was then employed to obtain the refined connector. The design framework has the ability to produce designs with smooth and uninterrupted boundaries, making them highly compatible with traditional casting methods and effectively tackling the manufacturing challenges related to topology optimization. The numerical simulation results demonstrate that, in comparison to traditionally welded T-joints of the same size, the stress concentration factor of the optimized joints exhibits a significant reduction, accompanied by a notable disparity in stress distribution. Moreover, the impact of the thickness of the brace and the axial compression ratio on the stress concentration factor of the optimized joints was relatively insignificant. The stress concentration factor of the cast-steel joint was reduced by more than 84%, leading to a significant enhancement in fatigue performance.

Keywords: cast-steel joint; optimization design; shape parameterization; numerical analyses; stress concentration factor

check for updates

Academic Editor: Antonio Formisano

Received: 10 December 2024
Revised: 14 January 2025
Accepted: 16 January 2025
Published: 19 January 2025

Citation: Jiang, K.; Yang, Z.; Chen, J.; Lv, G.; Yu, H. Optimization of Cast-Steel Tubular Circular-Hollow-Section Connections Based on Depth-First Search Algorithm. *Buildings* **2025**, *15*, 286. https://doi.org/10.3390/buildings15020286

Copyright: © 2025 by the authors. Licensee MDPI, Basel, Switzerland. This article is an open access article distributed under the terms and conditions of the Creative Commons Attribution (CC BY) license (https://creativecommons.org/licenses/by/4.0/).

1. Introduction

Welded connections are extensively utilized in the construction of high-rise buildings, grid shell structural systems, and large-scale transmission towers [1,2]. A chord and brace in the same plane can be connected through T-type, Y-type, and K-type joints. The traditional method for connecting a chord and a brace is through welding, commonly known as a welded circular-hollow-section (CHS) joint in engineering [3,4]. However, the management of welding quality on weld surfaces located on welded joints in a three-dimensional environment can present challenges. In complex connection scenarios, cast-steel joints can serve as an alternative to on-site welding. The development of casting technology has made it possible to achieve complex geometric shapes and structures with free-form designs that were previously considered impossible using traditional approaches. Hence, the increasing architectural practice of utilizing casting technology and the on-site assembly of prefabricated components showcases significant promise owing to its remarkable manufacturing accuracy and product excellence [5,6]. The design methodology for the transition area of castings is often not well defined, as it relies on the dimensions and

visual aspects of the chord and brace rather than specific physical models. The production capacity of castings is restricted due to process limitations in the molds. However, casting remains suitable for large critical nodes that do not require mass production.

The application of the topology optimization technique has been utilized to enhance CHS joint design [7,8]. The utilization of topology optimization has the potential to improve the mechanical capabilities of joints; nevertheless, it is not devoid of apparent constraints. Topology optimization often generates intricate and complex shapes that pose challenges for traditional casting processes in terms of manufacturability, thus necessitating the utilization of 3D printing technology [9,10]. The combination of topology optimization and 3D printing technology facilitates the achievement of efficient joint manufacturing [11]. The optimization of nodes in a parameterized grid shell was achieved by Zuo et al. [12–14] through the utilization of a bi-directional evolutionary structural optimization (BESO) algorithm, and its feasibility was demonstrated by fabricating specimens using additive manufacturing technology. The utilization of 3D printing technology is necessary due to its ability to produce intricate shapes that are challenging to manufacture through traditional casting processes. The expense associated with metal 3D printing continues to be considerably greater in comparison to conventional casting techniques, while the utilization of large-scale 3D printing technology is still in an early developmental phase [15]. Moreover, the utilization of topology optimization might result in surface irregularities and minor concerns regarding structural details, thereby requiring comprehensive post-processing procedures to achieve practical and viable designs [16]. This procedure of post-processing has the potential to cause variations in the structure from its optimized state, consequently leading to escalated time and labor expenses linked to the design process. Additionally, the consideration of structural stress is crucial for designers using existing topology optimization methods. However, utilizing strain energy as the objective function remains a significant challenge [17,18]. Hence, it is viable to devise joints based on structural stress analysis. Seifi et al. [19] employed the transition zone method and BESO technique to optimize joints within a shell structure, effectively reducing the stress concentration factor (SCF). The optimization technique employed by Li et al. [20], which combines the segmentation surface method with a genetic algorithm, resulted in a remarkable 39.2% reduction in the volume of three branch connectors within a tree-like structure, accompanied by a significant decrease in structural stress of 49.0%. Residual stresses are internal stresses that remain in a casting after solidification and cooling. These stresses can interact with the applied loads, leading to local stress amplification. Residual stresses can also affect a material's mechanical properties, such as its yield strength and ductility. In regions with high residual tensile stresses, a material may be more prone to plastic deformation and crack initiation, which can further increase the SCF. To mitigate the impact of residual stresses, design modifications such as implementing smooth geometric transitions and ensuring uniform wall thickness can be employed. Post-processing techniques (e.g., heat treatment, shot peening, and vibratory stress relief) can further reduce residual stresses.

In summary, the nodes derived from the topological optimization method are not conducive to traditional casting processes. Moreover, utilizing 3D printing for these nodes leads to prohibitively high costs. Consequently, optimizing regular curved surfaces that are compatible with traditional casting processes presents a significant contemporary challenge. Given the restricted availability of testing resources and the consequent elevated costs, utilizing the finite element (FE) method becomes particularly advantageous for investigating the mechanical characteristics of specimens [21,22]. In addressing fatigue issues for cast-steel joints on large-scale offshore electrical platforms operating at water depths exceeding one hundred meters, there is an urgent need to propose an optimized joint design during the component design phase. This study presents independently

designed and manufactured casting joints, which were optimized using a depth-first search (DFS) algorithm and computer-aided design software to effectively address the aforementioned issues. Compared to genetic algorithms and BESO, a DFS is relatively simple and straightforward to implement. Constraints can easily be incorporated into the DFS algorithm. When exploring a path, if a node violates a constraint, the algorithm can simply backtrack and explore another path. This makes it straightforward to handle hard constraints. A DFS is well suited for problems where the search space can be represented as a tree or a graph and the goal is to find a specific path or solution within that structure. A flowchart illustrating the design framework proposed in this study is depicted in Figure 1. The design framework will be structured as follows:

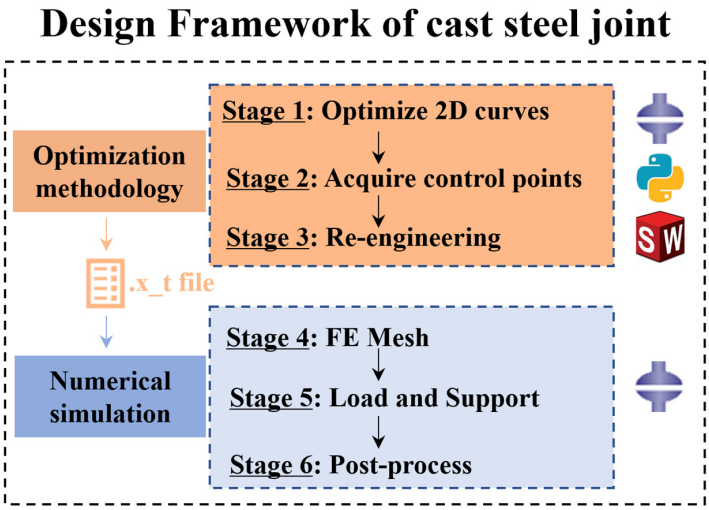


Figure 1. Diagram of design framework.

Firstly, by utilizing simple curves to establish connections between the chord and the brace in two dimensions, stress distribution patterns were investigated under various forms of simple curves.

Secondly, the selected simple curves were divided into equal central angles, and a depth-first search algorithm was employed to obtain the optimal combination of circular arcs, which then replaced the original simple curves.

Then, the optimized curve was associated with control points located in a three-dimensional space. However, the collection of these control points would result in a coarse surface, which is not suitable for direct manufacturing purposes. Therefore, the computer-aided design software Solidworks 2012 was utilized for re-engineering design, wherein non-uniform spline curves were employed to interconnect the control points.

Finally, the '.X_T' file generated by Solidworks was imported into large-scale finite element (FE) analysis software to establish an optimized node FE model, aiming to facilitate the investigation of strain distribution at optimized nodes and validate the effectiveness of the T-joint optimization method.

Stress concentration factors were compared between optimized nodes and conventional welded T-joints in order to provide a clear distinction. Ultimately, the main conclusions of this study were condensed, and potential avenues for future investigation were deliberated.

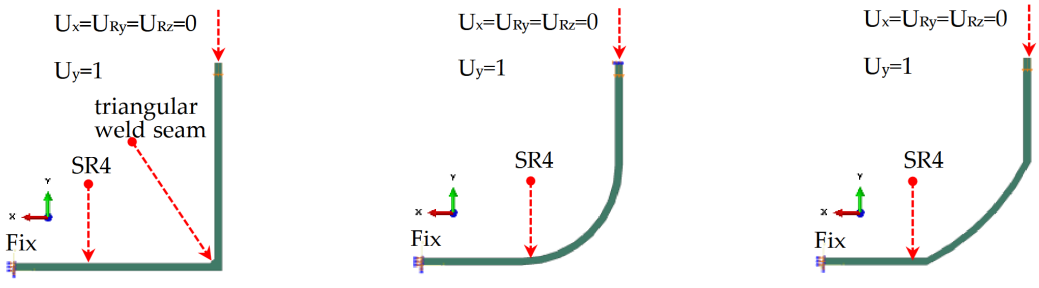
2. Optimization Methodology

The optimization framework for steel casting T-nodes comprises five primary modules: a selection module, an optimization algorithm module, and geometric modeling and numerical analysis modules. As illustrated in Figure 1, the procedure is as follows:

1. The selection module determines the fundamental 2D linear shape by analyzing the impact of stress distribution on two-dimensional simple line shapes.
2. The optimization algorithm module utilizes a depth-first search algorithm to generate optimized combinations and exports the optimized geometric parameters as a ".py" file to determine the coordinates of control points.
3. Subsequently, the module for geometric modeling carries out the processing of the ".py" file and generates the joint model as a ".x_t" file, following the specific guidelines provided in Section 2.2.
4. A module for conducting numerical simulation analysis is employed, and the outcomes are exported in the format of ".xls" files to be utilized in the SCF analysis module (see Section 2.3).
5. The applicability of the optimization framework is analyzed based on a comprehensive analysis of the stress concentration factor analysis module (refer to Section 3.2 for detailed information).

2.1. Module Selection

The stress transmission behavior in T-shaped shells constructed with different curves was investigated using ABAQUS 6.14 software [23]. As depicted in Figure 2, S4R elements were employed for simulating shells. Actual welded joints often have a triangular weld seam; thus, the right-angle shell model incorporates triangular weld seams in the corner areas. In accordance with the principle of 'equivalent strength' between welds and base materials specified in [24], the weld seam and the right-angled shell were modeled as a unified entity, as depicted in Figure 2a. As shown in Figure 2b, shells that are perpendicular to each other are connected by arcs, where the radius of each arc is equal to half of the length of the side, forming a right-angle shell model. Additionally, these arcs are tangent to the shells that are perpendicular. As illustrated in Figure 2c, the stress transmission behavior was analyzed by introducing a non-tangent circular arc to connect the sides in the right-angle shell model. The radius of this circular arc is 0.707 times that of the side. The material properties of a conventional cast-steel joint were utilized as the material characteristics for the T-shaped shell model. The grid control size was determined using tetrahedral meshing and scanning techniques for grid generation, with a focus on sensitivity analysis to refine the corner regions. The horizontal legs of the right angle were subjected to fixed boundary conditions, while a downward pressure was applied to the vertical leg. After conducting the numerical analysis, a post-processing script was utilized to gather the maximum stress response data along the inner path of the right-angle side. The stress undergoes a significant alteration when any non-rounded area is present, as depicted in Figure 3. Conversely, the utilization of rounded arc transition areas facilitates a gradual change in stress. The present study therefore employed the utilization of arcs as the connecting method for the transition zone in T-shaped cast-steel nodes.



(**a**) Right angle (**b**) 1/4 Arc-tangent (**c**) Arc-No tangent

Figure 2. Schematic view of the FE model.

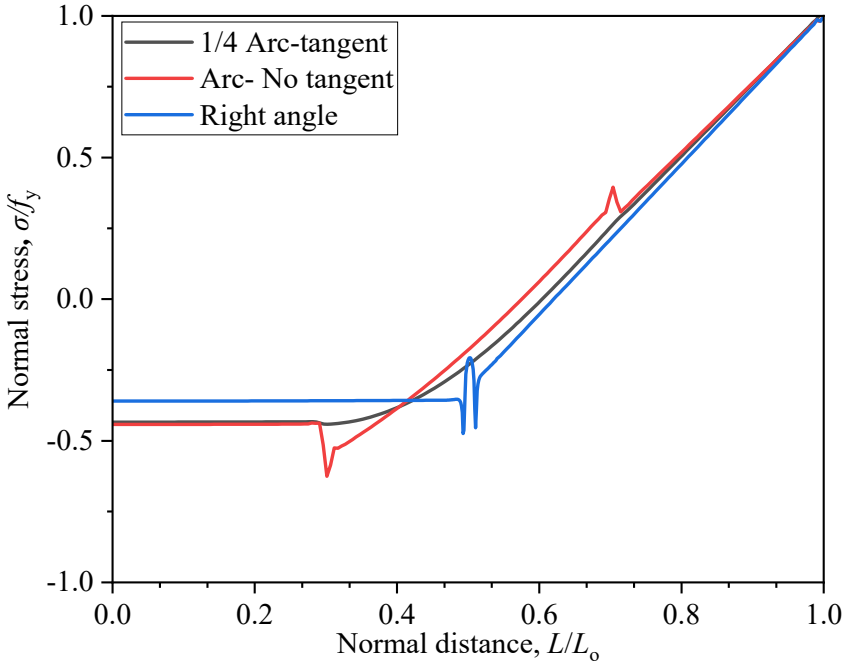


Figure 3. The Mises stress of the optimized curves.

2.2. Optimization Algorithm

To achieve the optimal stress transfer path, a depth-first search algorithm was utilized to explore the most effective combination of circular arcs. Implementation path: Firstly, the initial circular arc was discretized into a finite number of segments, n, based on a predetermined central angle. Secondly, the i-th arc was replaced with different arcs that adhere to the principles of having equal central angles and being tangent to each other. Subsequently, a depth-first search algorithm was employed to merge the arcs, ensuring that the merged targets satisfied the prerequisite of the final arc segment returning to the endpoint of the initial arc. Finally, by subjecting the combination arcs that met the requirements to identical load and boundary conditions, the combination arc with the lowest stress gradient was identified based on the output stress response data, and the corresponding information regarding its geometric parameters was exported.

The computational cost of the DFS algorithm is shown in Figure 4. To compare the computational efficiency of the DFS algorithm, a CPU speed of 4 cores per hour was used to execute the DFS algorithm. It can be seen that using various segments had little effect on the stress gradient; however, an increase in the number of segments resulted in longer computation times. Considering an optimal balance between high accuracy and computational efficiency, the algorithm was configured with a segment size of 10.

2.3. Geometric Model Construction

SolidWorks software was utilized for the geometric modeling of cast-steel nodes. The 3D CADsoftware SolidWorks 2012 is widely utilized in the domains of mechanical design and engineering due to its exceptional power and capabilities. The built-in API interface of Python allows for secondary development, empowering users to accomplish automated design and data processing tasks with proficiency. To determine the initial geometric parameters of the initial single arc, the chord and brace can be sectioned by the reference plane passing through the axis of the brace. The geometric relationship between the chord wall and the brace wall can be categorized into three types: (a) when both the chord and the brace are sectioned by a reference plane that passes through their respective axes, the extension lines of the chord wall and the brace wall are perpendicular to each other;

(b) when the chord and the brace are sectioned by a reference plane that passes through the axis of the brace and is perpendicular to the axis of the chord, the chord has an annular cross-section; (c) apart from these two scenarios, when the chord and the brace are sectioned by a reference plane that passes through the axis of the brace, the chord has an elliptical ring cross-section. The outer perimeters of the various chord cross-sections obtained were projected onto a common plane, which serves as a reference plane, intersecting both the axis of the brace and the axis of the chord, as illustrated in Figure 5.

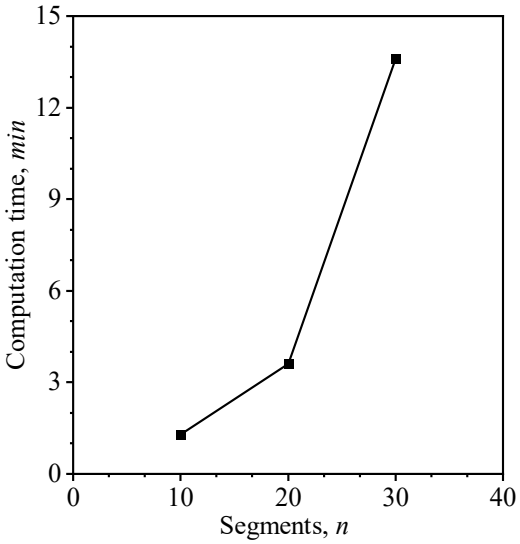


Figure 4. The computational cost of the DFS algorithm.

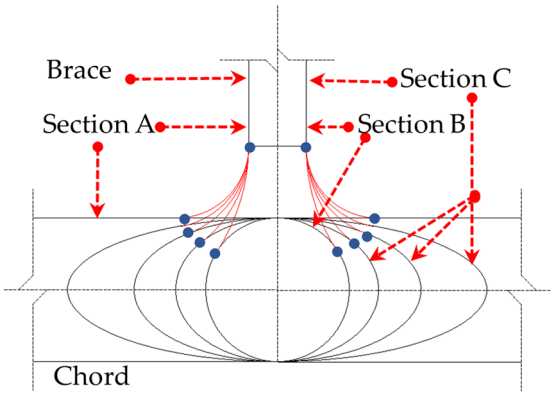


Figure 5. Initial geometric parameters.

The specific spatial coordinates for optimizing the control points of circular arcs can be determined by transforming geometric parameter information for a two-dimensional composite arc into three-dimensional space coordinates using the cylindrical coordinate transformation formula. The generation of the optimized zone in the cast-steel node is jointly controlled by the inner and outer surfaces of the chord and the brace. Two methods can be used to construct it:

(a) Firstly, separately establish the outer surface of the chord, the outer surface of the transition zone, the outer surface of the brace, and the end face. Then, stitch these three parts together and fill them internally to obtain a solid model X. Similarly, construct a solid model Y consisting of the inner surface of the chord, the inner surface

of the optimized zone, the inner surface of the brace, and the end face. Perform Boolean operations on these two models to generate cast-steel nodes.

(b) A cast-steel node comprises three components: the chord, the brace, and the optimized zone. Since both the chord and the brace are made from steel tubes, which can be generated based on their axis lines and diameter and wall thickness parameters, only the part inside the optimized area should be cut off for both the chord and the brace. The components in the optimized area can be generated by constructing their inner and outer surfaces and end face and then stitching them together. The latter approach was employed in this study for the purpose of geometric modeling.

3. Numerical Example

3.1. T-Joint

3.1.1. Joint Configuration

The T-shaped node is a commonly encountered configuration in cast-steel nodes. Figure 6 illustrates the geometric parameters of the node. The connection consists of two components: the chord measures D300 × 8 × 540 mm, while the brace measures D113 × 8 × 350 mm. The static analysis in this paper assumes that the loads are applied slowly and steadily and there are no time-dependent effects. These assumptions are valid for many situations where the loading is relatively static or the dynamic effects are negligible. However, in the case of fatigue and impact loading, the dynamic nature of the loads cannot be ignored. A static analysis will not be able to accurately predict the stress concentration factor under these dynamic loading conditions. Figure 7 illustrates the loading and boundary conditions, wherein fixed supports are present at both ends of the chord. The end of the brace is coupled with a reference point, where a concentrated force is applied. This arrangement ensures that a uniformly distributed load effectively acts on the end of the brace. During the loading of the brace, the node must remain within its elastic limit, thereby limiting the magnitude of the applied load. The T-shaped node was subjected to a gradually increasing load of $0.1 f_y A_{s,b}$ until it reached the yield stress, which is considered the maximum load (N_u) for the joint. Subsequently, the final load applied for determining the stress concentration factor was $0.5N_u$ [25].

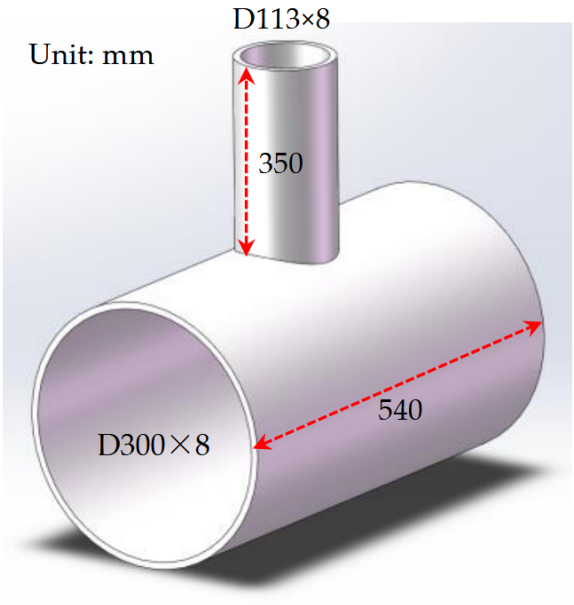


Figure 6. Geometric parameters of the T-joint.

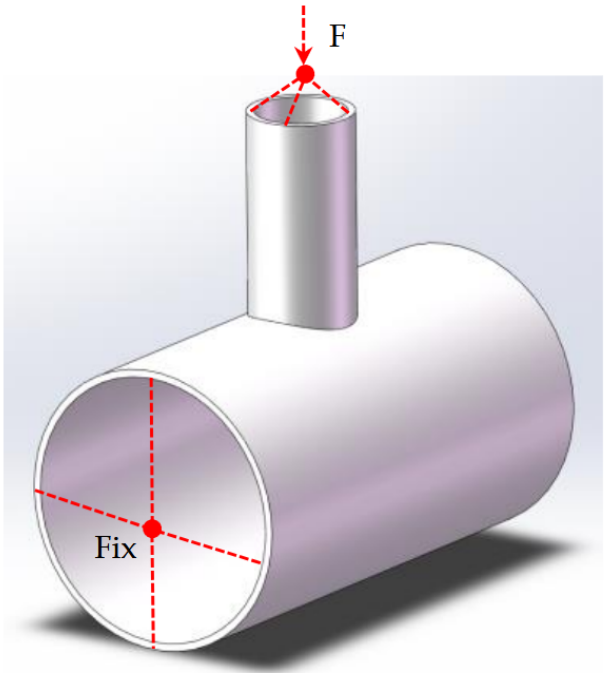


Figure 7. Loading conditions and boundary conditions.

3.1.2. Solid Modeling

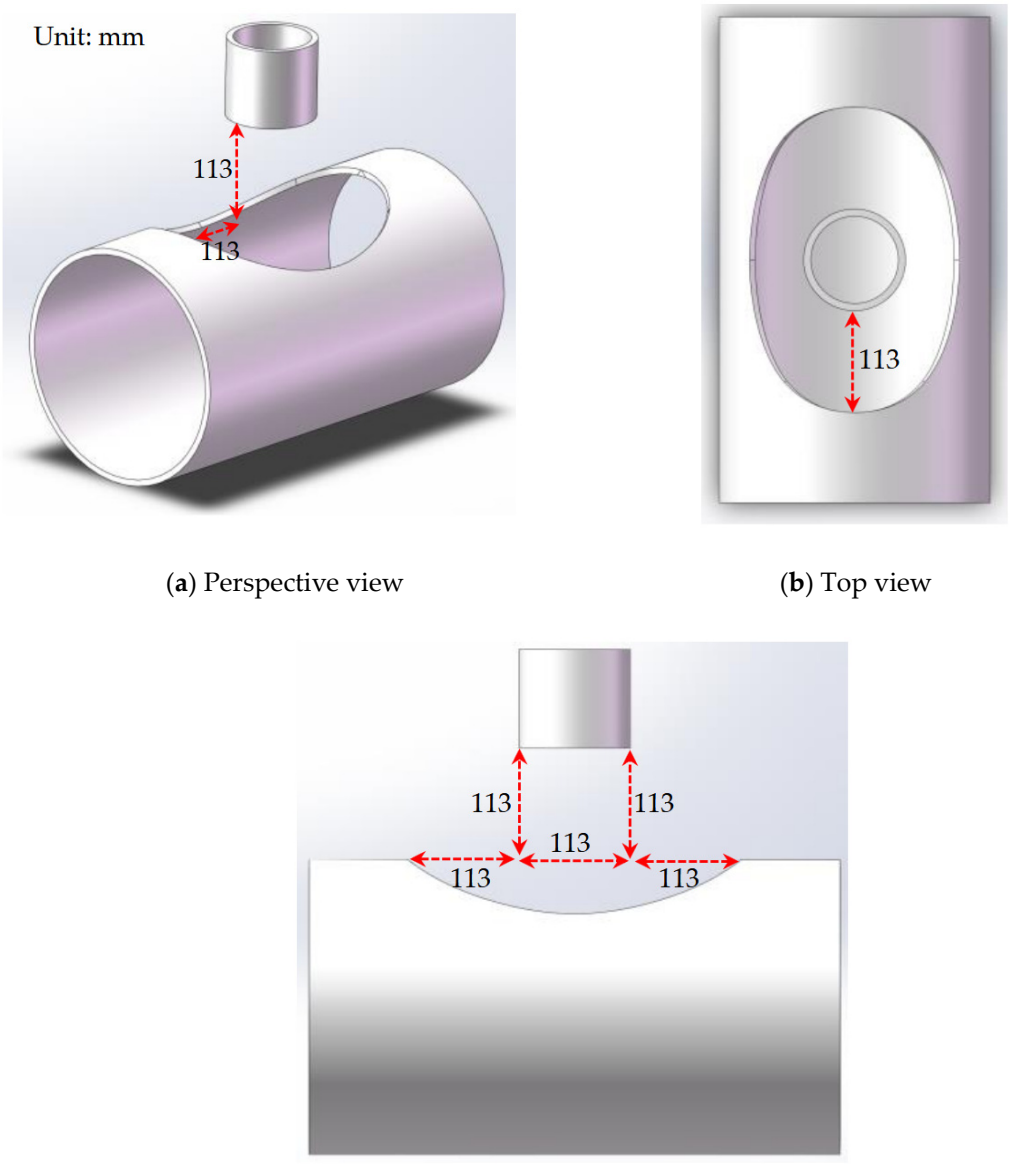
The brace and chord were initially created in SolidWorks, utilizing the geometric modeling methods discussed in Section 2.3. To ensure a balance between material usage and stress concentration factors, the cutting area was determined based on the diameter of the brace, as illustrated in Figure 8. The T-shaped cast-steel joint exhibits symmetry, allowing for the creation of a simplified 1/4 model in the calculations. Consequently, a ".x_t" file was generated, as depicted in Figure 8. The joint depicted in Figure 9 was designated RE1. Additionally, the joint RE2 was constructed to analyze the impact of the brace wall on this new type of node. The dimensions of the brace in specimen RE2 are D113 × 6 × 350 mm. The key characteristics of the specimens are presented in Table 1.

3.1.3. FE Modeling

The numerical simulation analysis module was run through the secondary development of Abaqus software. Firstly, the model generated by the geometric modeling module was imported, and then the joint's material properties were established. The selected joint material is cast steel [20], as presented in Table 2. The generation of the grid was facilitated by employing the tetrahedral mesh and scanning method, with the determination of the grid control size being based on sensitivity analysis. Fixed boundaries were implemented at the ends of the chord, whereas the end faces of the brace were connected to a reference point. A final load ($0.5N_u$) was applied at the reference point. Upon completion of the numerical analysis, a post-processing script was implemented to gather crucial structural response data, encompassing the maximum stress (σ_{max}) of the optimized region and chord across various cross-sections. The extracted data were subsequently utilized to calculate the stress concentration factor. The stress concentration factor can be determined based on Equation (1), considering the simplicity of the model and the elastic behavior of the cast steel [26].

$$\eta_{SCF} = \frac{\sigma_{max}}{\sigma_n} \quad (1)$$

where σ_n denotes the nominal stress of the brace.



(**a**) Perspective view (**b**) Top view

(**c**) Main view

Figure 8. Optimized region of the T-joint.

Table 1. The key characteristics of the specimens.

ID	Chord			Brace			Type
	D_0 (mm)	t_0 (mm)	l_0 (mm)	D_1 (mm)	t_1 (mm)	l_1 (mm)	
T	300	8	540	113	8	350	Welded T-joint
RE 1	300	8	540	113	8	237	Optimized T-joint
RE 2	300	8	540	113	6	237	Optimized T-joint

Table 2. Material properties of joints.

Type	Elastic Modulus (MPa)	Yield Strength (MPa)	Density (kg/m^3)	Poisson's Ratio
Cast steel	2.06×10^5	235	7850	0.3

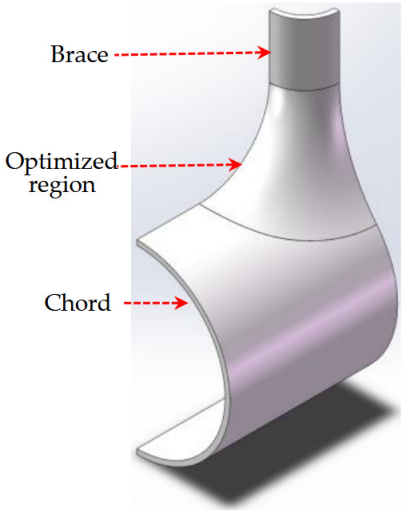


Figure 9. Model.

3.2. Modeling Results and Discussion

The objective of this study is to investigate the disparity between the stress concentration factors of optimized joints and welded T-joints. The model for the welded joint encompasses not only the chord and brace but also the weld seam, with the size of the weld seam being determined in accordance with reference [24]. The stress distributions of the welded T-shaped joint and the optimized T-shaped node exhibit a noticeable disparity, as depicted in Figures 10 and 11. The phenomenon of stress concentration in the optimized T-joints is not obvious, but it is primarily distributed on the outer surface of the lower part of the optimized region and on the inner surface of the adjacent chord connected to the optimized area.

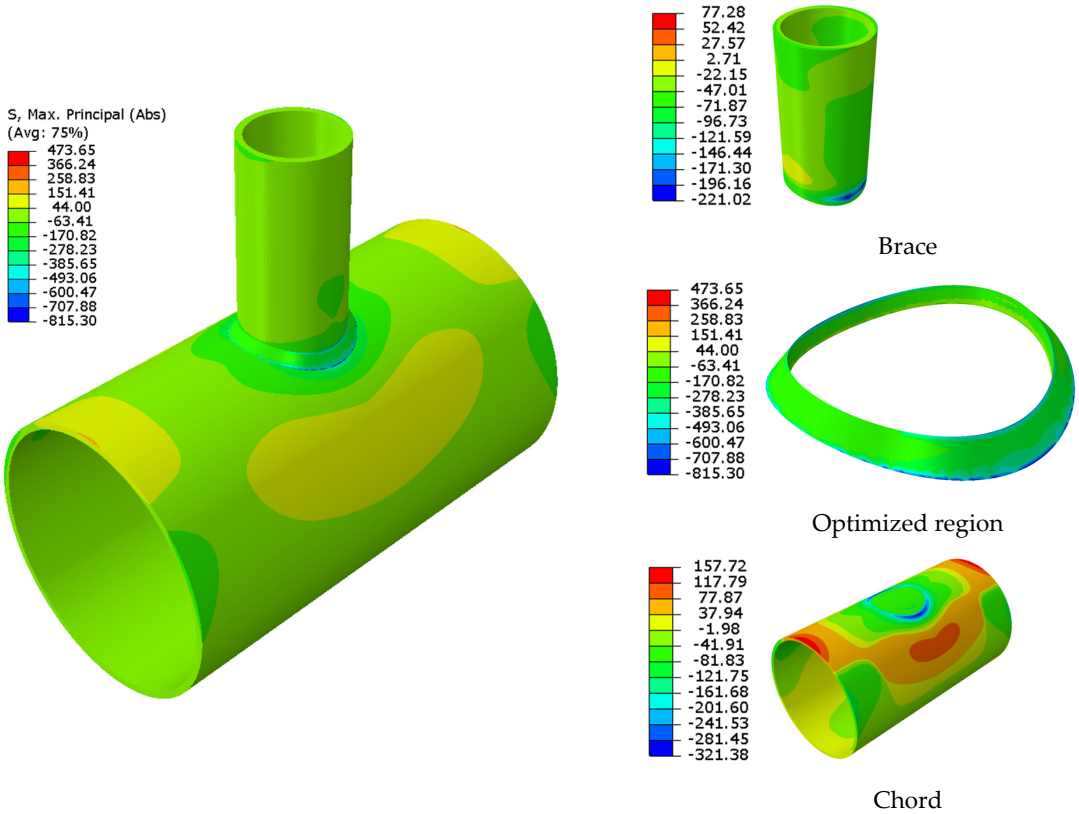
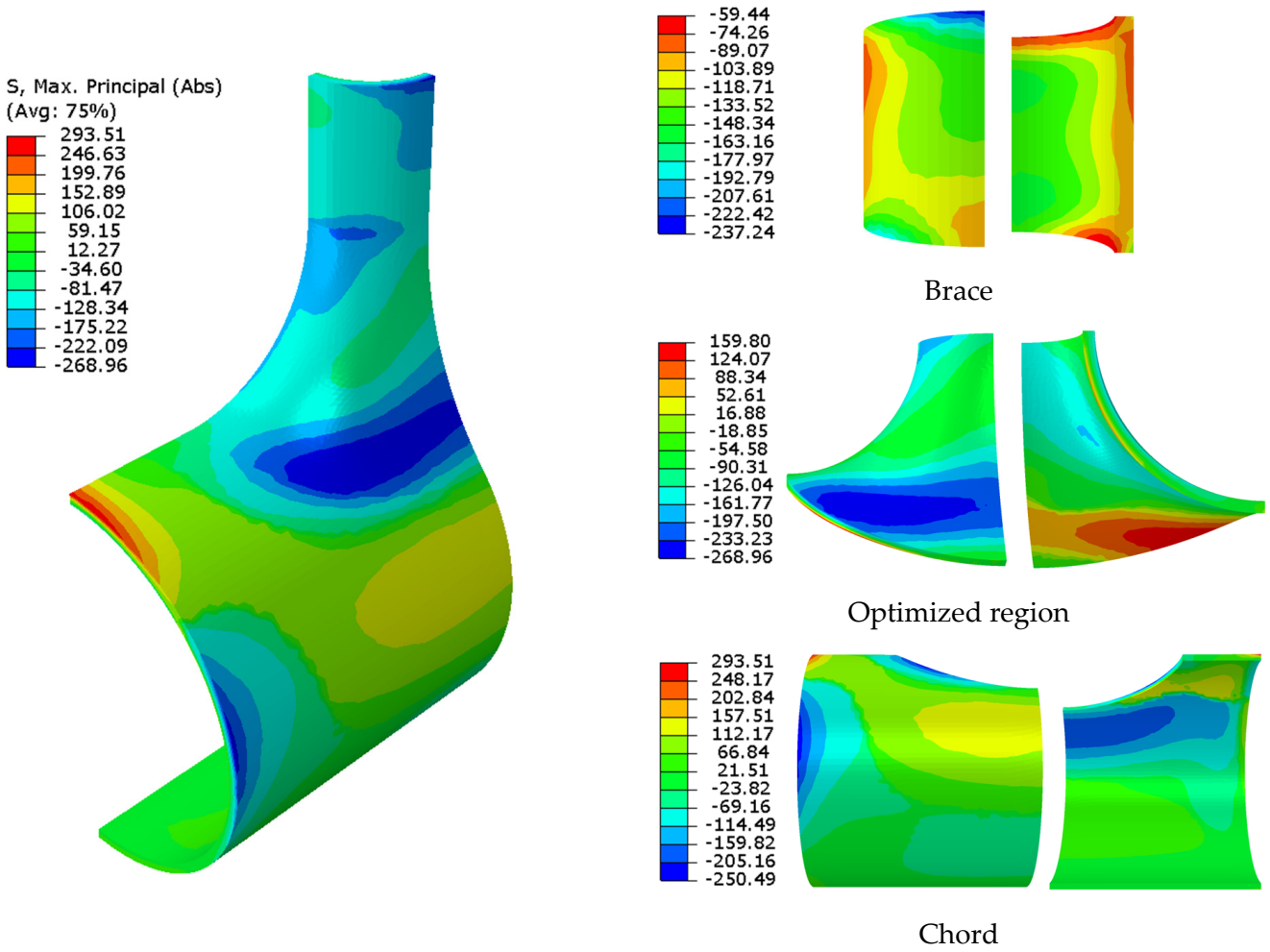


Figure 10. Max principal stress of welded T-joint.



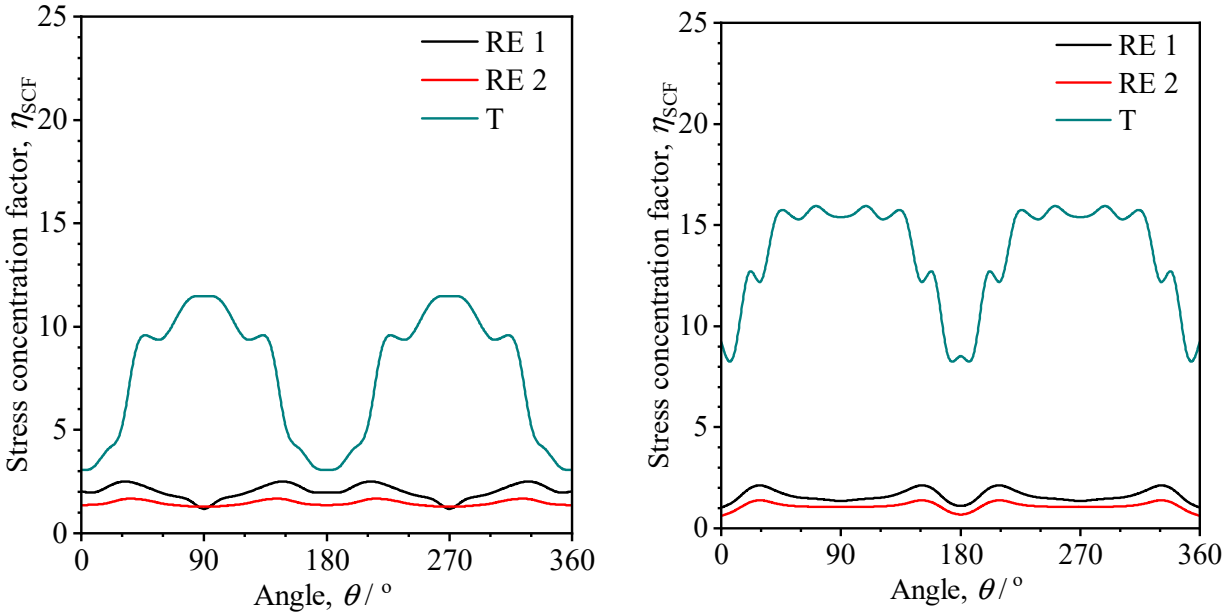
(**a**) Perspective view (**b**) Main View and back view

Figure 11. Max principal stress of optimized T-joints.

The stress concentration factor of a new type of T-shaped joint was studied by setting a reference plane that passes through both the axis of the brace and the axis of the chord. The angle θ is defined as the angle between the reference plane and plane that passes through the axis of the brace. A separate analysis was conducted on the stress concentration factors for various cross-sections of the chord and optimization region.

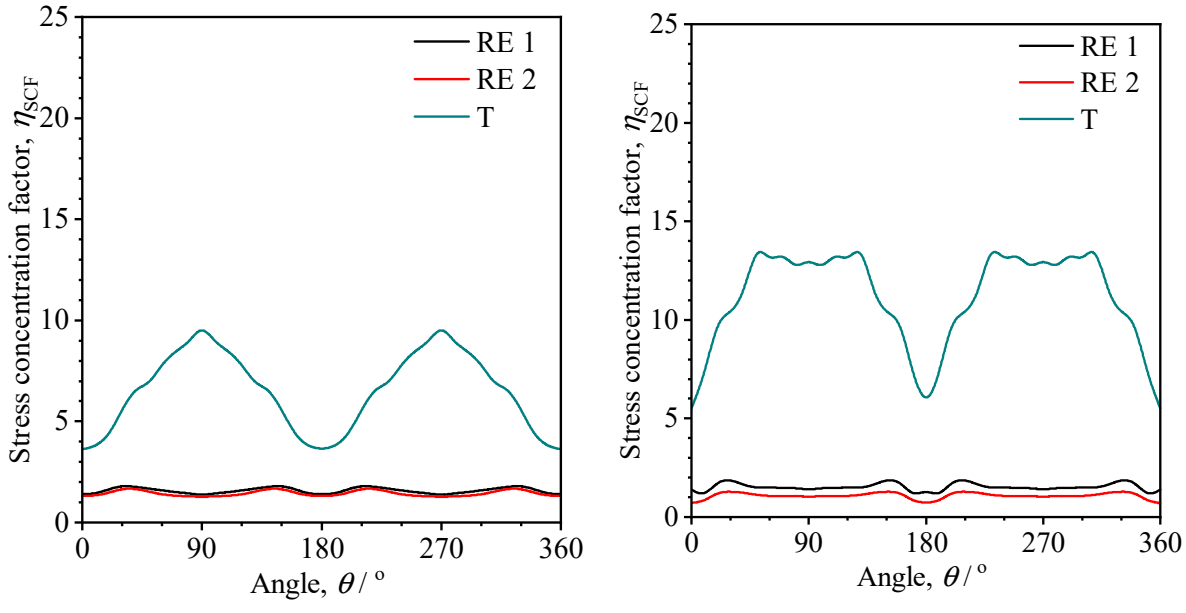
3.2.1. Axial Load

The optimized T-shaped cast-steel joint exhibits a significantly lower stress concentration factor compared to the welded T-shaped node when subjected to tensile and compressive loads, as is evident from Figures 12 and 13. The distribution of the stress concentration factors of the optimized joint is remarkably uniform, with a prominent hot spot located at approximately $\theta = 30°$. The stress concentration factors for both tensile and compressive loads in the optimized T-shaped cast-steel joints are essentially identical. Hence, when analyzing stress concentration factors, it suffices to select a single load condition analysis. The stress concentration factor of the optimized T-shaped cast-steel joint can be further reduced by decreasing the thickness of the brace. However, this reduction is limited due to the already low overall stress concentration factor of the joint.



(**a**) Optimized region (**b**) Chord

Figure 12. Distribution of η_{SCF} of joints under axial compression.



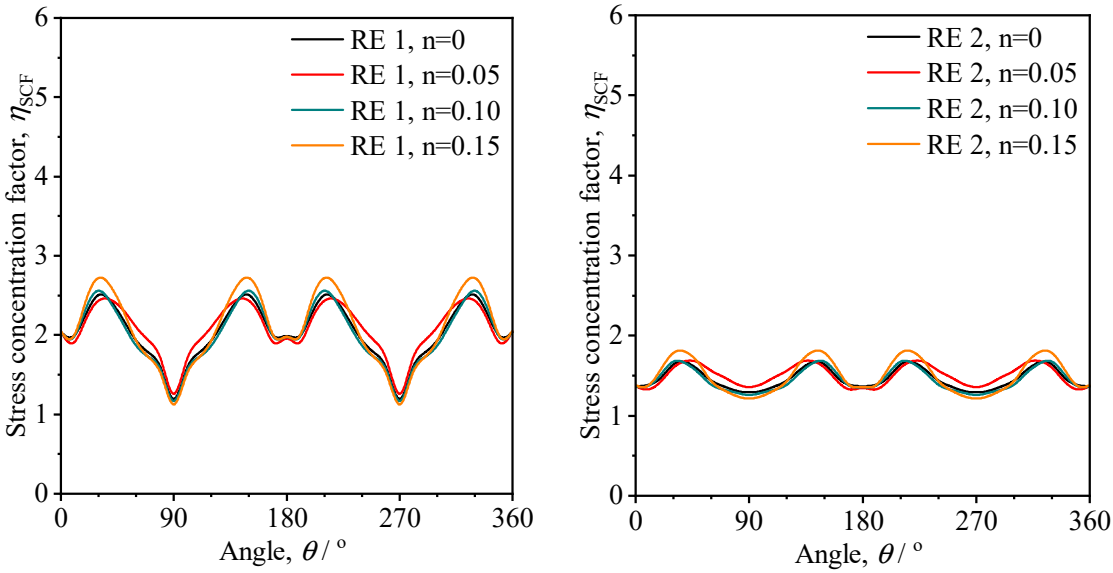
(**a**) Optimized region (**b**) Chord

Figure 13. Distribution of η_{SCF} of joints under axial tension.

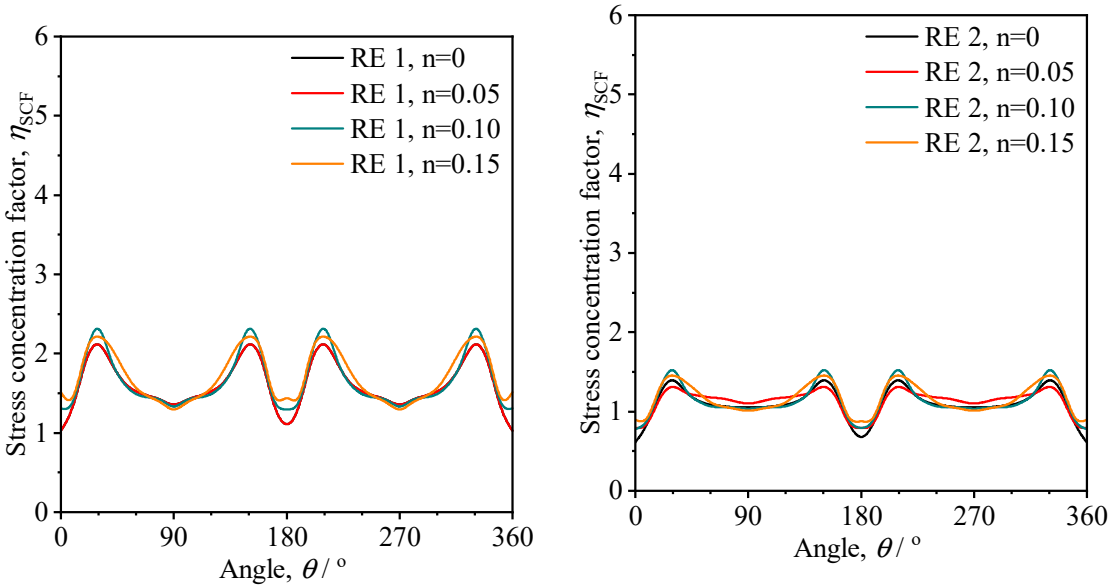
3.2.2. The Effect of the Axial Compression Ratio on η_{SCF}

The effect of the axial compression ratio on the stress concentration factor in the optimized joints was investigated by applying a specific axial load to the end of the chord. Stress concentration factors were then tested under different tension and compression conditions at various axial compression ratios. The results are presented in Figures 14 and 15. The results indicate that the axial compression ratio has minimal impact on the stress concentration coefficient distribution for the optimized region under different cross-sections, as well as on the chord's stress concentration coefficient. This is attributed to the fact that, in comparison with conventional nodes, the optimized nodes exhibit a notably greater stress

concentration region. Under axial tensile loading, an increase in the axial compression ratio leads to a slight decrease in the stress concentration factor of the chord. Conversely, under axial compressive loading, an increase in the axial compression ratio results in a slight increase in the stress concentration factor of the chord. The compressive stress concentration factor of the node under axial tensile loading is reduced by the axial compression ratio, thereby enhancing structural safety. However, given its limited impact, it can be disregarded in fatigue design. The stress concentration factor of the compressed node reaches a peak amplitude of 8.5% when the axial stress ratio is 0.15. In large-span or heavily loaded structures, the chord often experiences significant axial loads. Neglecting the influence of the axial compression ratio can potentially compromise structural integrity and pose safety hazards. Hence, the influence of the axis compression ratio should be taken into account when configuring the fatigue design of optimized joints, particularly in the calculation of the stress concentration factor under axial loads.

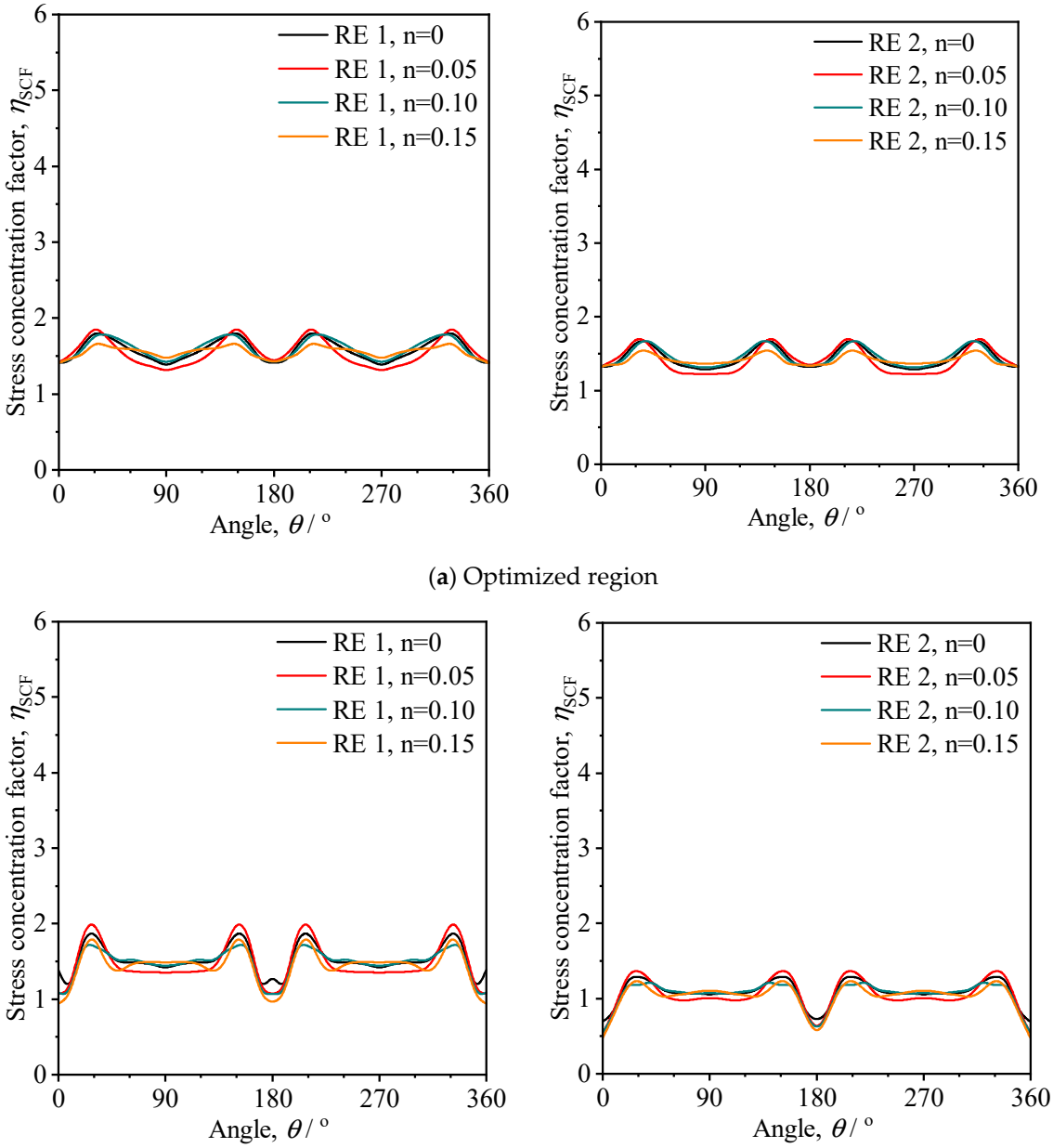


(**a**) Optimized region



(**b**) Chord

Figure 14. Distribution of η_{SCF} of joints under axial compression at various axial compression ratios.



(**a**) Optimized region

(**b**) Chord

Figure 15. Distribution of η_{SCF} of joints under axial tension at various axial compression ratios.

3.2.3. Max Stress Concentration Factor, $\eta_{SCF,max}$, of Joints

Current specifications, including the API Standard [27], LR Guide [28,29], and DNV manual [30], have provided methodologies for predicting the maximum stress concentration factor. A comparison between the SCF simulation results of the T-welded joint and predictions from various specifications is presented in Table 3. It is evident that the developed T-welded joint model is effective in predicting the maximum stress concentration factor.

Table 3. Comparison of max stress concentration factor of weld joints between FE results and design predictions (API, DNV, and LR).

ID	FE	API	DNV	LR
T	16.3	11.8	16.4	9.0

The stress concentration factors of all models are compared based on the numerical results, as presented in Table 4. It can be observed that the optimized nodes exhibit a significant reduction in maximum stress concentration factors under axial compression and axial tension conditions, with decreases of 84.1% and 85.6%, respectively, compared to the welded joints. The maximum stress concentration factors of the optimized nodes decreased by 34.9% and 13.0% under axial compression and tension conditions, respectively, when the thickness of the brace was reduced, and it was observed that increasing the axial compression ratio did not significantly impact the magnitude of this reduction.

Table 4. Max stress concentration factor of joints.

ID	Load Type	Axial Compression Ratio on the Chord	$\eta_{SCF,Max}$
T	Compression	0	16.3
	Tension	0	13.4
RE 1	Compression	0	2.58
		0.05	2.47
		0.10	2.64
		0.15	2.80
	Tension	0	1.93
		0.05	2.07
		0.10	1.79
		0.15	1.69
RE 2	Compression	0	1.68
		0.05	1.70
		0.10	1.72
		0.15	1.82
	Tension	0	1.68
		0.05	1.74
		0.10	1.70
		0.15	1.56

4. Conclusions

The present study investigated a novel optimization method and applied it to a cast-steel T-joint, which was validated using the FE model. The main conclusions can be summarized as follows:

(1) The method proposed incorporates five fundamental modules: a selection module, an optimization algorithm module, a geometric modeling module, and a numerical analysis module. A basic connection method for joints was determined using a depth-first search algorithm, while parameterized modeling and analysis were conducted using Solidworks and Abaqus.

(2) Compared to welded T-joints, this optimized method offers several advantages. It can significantly reduce stress concentration factors and create a more uniform stress distribution in the optimized zone, thereby facilitating efficient design solutions.

(3) Under axial tensile loading, increasing the axial compression ratio slightly decreases the stress concentration factor of the chord in the optimized joint. Conversely, under axial compressive loading, increasing the axial compression ratio slightly increases this factor.

(4) The optimization algorithm for 2D curves has demonstrated benefits; however, further research is required to comprehend the impact of optimizing these curves on stress effects in a three-dimensional space, aiming to achieve more efficient solutions.

Author Contributions: Conceptualization, Z.Y.; methodology, Z.Y.; software, K.J.; validation, K.J., J.C. and G.L.; formal analysis, Z.Y.; investigation, Z.Y.; resources, Z.Y.; data curation, Z.Y.; writing—original draft preparation, Z.Y.; writing—review and editing, J.C.; visualization, J.C.; supervision, G.L.; project administration, H.Y.; funding acquisition, K.J. All authors have read and agreed to the published version of the manuscript.

Funding: This work was supported by the Project of Power China Huadong Engineering Corporation Limited (HDY-CGHT17-20240304Y).

Data Availability Statement: The data will be made available upon request.

Conflicts of Interest: The authors declare no conflicts of interest.

References

1. Xia, Q.; Ma, L.; Li, G.; Hu, C.; Zhang, L.; Xu, F.; Liu, Z.H. Stress Concentration Factors of Concrete-Filled Double-Skin Tubular K-Joints. *Buildings* **2024**, *14*, 1363. [CrossRef]
2. Zheng, J.; Nakamura, S.; Ge, Y.; Chen, K.; Wu, Q. Formulation of stress concentration factors for concrete-filled steel tubular (CFST) T-joints under axial force in the brace. *Eng. Struct.* **2018**, *170*, 103–117. [CrossRef]
3. Xu, F.; Zhou, X.; Chen, J.B.; Wang, Y.H.; Zhao, J. Plastic and punching shear strengths of concrete-filled steel tubular gapped K-joints without noding eccentricity under brace axial loading. *Thin-Walled Struct.* **2024**, 112139. [CrossRef]
4. Xu, F.; Chen, J.; Jin, W.-L. Experimental investigation of SCF distribution for thin-walled concrete-filled CHS joints under axial tension loading. *Thin-Walled Struct.* **2015**, *93*, 149–157. [CrossRef]
5. Wei, Z.; Pei, X.; Jin, H. Evaluation of welded cast steel joint fatigue data using structural stress methods. *J. Constr. Steel Res.* **2021**, *186*, 106895. [CrossRef]
6. Du, W.; Sun, Y.; Yang, M. Bearing capacity of the cast-steel joint with branches under eccentric load. *J. Constr. Steel Res.* **2017**, *135*, 285–291. [CrossRef]
7. Zhu, J.H.; Zhang, W.H.; Xia, L. Topology optimization in aircraft and aerospace structures design. *Arch. Comput. Methods Eng.* **2016**, *23*, 595–622. [CrossRef]
8. Shi, G.; Guan, C.; Quan, D.; Wu, D.; Tang, L.; Gao, T. An aerospace bracket designed by thermo-elastic topology optimization and manufactured by additive manufacturing. *Chin. J. Aeronaut.* **2020**, *33*, 1252–1259. [CrossRef]
9. Hadjipantelis, N.; Weber, B.; Buchanan, C.; Gardner, L. Description of anisotropic material response of wire and arc additively manufactured thin-walled stainless steel elements. *Thin-Walled Struct.* **2022**, *171*, 108634. [CrossRef]
10. Yan, J.J.; Chen, M.T.; Quach, W.M.; Yan, M.; Young, B. Mechanical properties and cross-sectional behavior of additively manufactured high strength steel tubular sections. *Thin-Walled Struct.* **2019**, *144*, 106. [CrossRef]
11. Buchanan, C.; Gardner, L. Metal 3D printing in construction: A review of methods, research, applications, opportunities and challenges. *Eng. Struct.* **2019**, *180*, 332–348. [CrossRef]
12. Zuo, W.K.; Chen, M.T.; Chen, Y.Y.; Zhao, O.; Cheng, B.; Zhao, J.C. Additive manufacturing oriented parametric topology optimization design and numerical analysis of steel joints in gridshell structures. *Thin-Walled Struct.* **2023**, *188*, 110817. [CrossRef]
13. Chen, M.-T.; Zuo, W.; Huang, Y.; Cheng, B.; Zhao, J. Novel Paradigm for Steel Joints in Gridshell Structures: From Structural Optimization to Advanced Construction. *Ce/Papers* **2023**, *6*, 781–787. [CrossRef]
14. Chen, M.-T.; Zuo, W.; Chen, Y.; Zhao, O.; Cheng, B.; Zhao, J. Parametric topology optimization design and analysis of additively manufactured joints in spatial grid structures. *Eng. Struct.* **2024**, *300*, 117123. [CrossRef]
15. Wang, L.; Du, W.; He, P.; Yang, M. Topology optimization and 3D printing of three-branch joints in treelike structures. *J. Struct. Eng.* **2020**, *146*, 04019167. [CrossRef]
16. Subedi, S.C.; Verma, C.S.; Suresh, K. A review of methods for the geometric post-processing of topology optimized models. *J. Comput. Inf. Sci. Eng.* **2020**, *20*, 060801. [CrossRef]
17. Xia, L.; Zhang, L.; Xia, Q.; Shi, T. Stress-based topology optimization using bi-directional evolutionary structural optimization method. *Comput. Methods Appl. Mech. Eng.* **2018**, *333*, 356–370. [CrossRef]
18. Fan, Z.; Xia, L.; Lai, W.; Xia, Q.; Shi, T. Evolutionary topology optimization of continuum structures with stress constraints. *Struct. Multidiscip. Optim.* **2019**, *59*, 647–658. [CrossRef]
19. Seifi, H.; Rezaee Javan, A.; Xu, S.; Zhao, Y.; Xie, Y.M. Design optimization and additive manufacturing of nodes in gridshell structures. *Eng. Struct.* **2018**, *160*, 161–170. [CrossRef]
20. Li, G.; Li, Z.; Zeng, Q.; Guo, X. Shape optimization of cast steel tubular joints based on subdivision surface and genetic algorithm. *Thin-Walled Struct.* **2024**, *204*, 112258. [CrossRef]
21. Wang, Z.; Yuan, Y.; Zhang, S.; Lin, Y.; Tan, J. A multi-state fusion informer integrating transfer learning for metal tube bending early wrinkling prediction. *Appl. Soft Comput.* **2024**, *151*, 110991. [CrossRef]

22. Wang, Z.; Wang, C.; Zhang, S.; Qiu, L.; Lin, Y.; Tan, J.; Sun, C. Towards high-accuracy axial springback: Mesh-based simulation of metal tube bending via geometry/process-integrated graph neural networks. *Expert Syst. Appl.* **2024**, *255*, 124577. [CrossRef]
23. *ABAQUS*, Version 6.14; ABAQUS Standard User's Manual; Dassault Systèmes Corporation: Providence, RI, USA, 2014.
24. Xu, F. Mechanical Behaviour of Concrete-Filled Thin-Walled Steel Tube Members and Connections. Ph.D. Thesis, Zhejiang University, Hangzhou, China, 2016.
25. Chen, J.; Nie, J.G.; Zhou, C.Y. Study on stress concentration factor of concrete-filled steel tubular T-joints. *J. Build. Struct.* **2018**, *39*, 149–157. (In Chinese)
26. Pandey, M.; Young, B. Stress concentration factors of cold-formed high strength steel tubular T-joints. *Thin-Walled Struct.* **2021**, *166*, 107996. [CrossRef]
27. API American Petroleum Institute. *Recommended Practice for Planning, Designing and Constructing Fixed Offshore Platforms*; API RP2A-LRFD; API American Petroleum Institute: Washington, DC, USA, 1993.
28. Smedley, P.A.; Fisher, P.J. A review of stress concentration factors for tubular complex joints. *Integr. Offshore Struct.* **1990**, *4*, 279.
29. Smedley, P.A.; Fisher, P.J. Stress concentration factors for simple tubular joints. In Proceedings of the First International Offshore and Polar Engineering Conference, ISOPE, Edinburgh, UK, 11–16 August 1991.
30. DNV. *DNV Recommended Practice RP-C203, Fatigue Strength Analysis of Offshore of Steel Structures*; Det Norske Veritas: Bærum, Norway, 2005.

Disclaimer/Publisher's Note: The statements, opinions and data contained in all publications are solely those of the individual author(s) and contributor(s) and not of MDPI and/or the editor(s). MDPI and/or the editor(s) disclaim responsibility for any injury to people or property resulting from any ideas, methods, instructions or products referred to in the content.